Proceedings of the ASME 2016 International Mechanical Engineering Congress & Exposition
IMECE 2016
November 11-17, 2016, Phoenix, USA

IMECE2016-66664

ON WIND-DRIVEN LAND VEHICLES

G. Reina[*]
Department of Engineering for Innovation
University of Salento
Lecce, Italy 73100
Email: giulio.reina@unisalento.it

M. M. Foglia
Department of Mechanical, Mathematics and Management Engineering
Politecnico of Bari
Bari, Italy 70125
Email: mm.foglia@poliba.it

ABSTRACT

This paper deals with the study of a land-yacht, that is a ground vehicle propelled by wind energy. There is a large interest in exploring alternative source of energy for propulsion and wind energy could be a feasible solution being totally green, available and free. The idea envisaged by a land-yacht is that of using one or several flexible or rigid vertical wing-sails to produce a thrust-force, which can eventually generate a higher travel velocity than its prevailing wind. A model of a three-wheel land-yacht is presented capturing the main dynamic and aerodynamic aspects of the system behaviour. Simulations are included showing how environment conditions, i.e. wind intensity and direction, influence the vehicle response and performance. In view of a robotic embodiment of the vehicle, a controller of the sail trim angle and front wheel steer angle is also discussed for autonomous navigation.

NOMENCLATURE

I_d Instantaneous center of rotation of the vehicle
G Center of mass
R Curvature radius
a Front pitch
b Rear pitch
l Vehicle pitch
t Vehicle width
δ Steer angle
α_A Slip angle of the front wheel
α_{PR} Slip angle of the rear right wheel
α_{PL} Slip angle of the rear left wheel
β Slip angle of the vehicle
v_G Vehicle velocity
u Longitudinal component of v_G
v Lateral component of v_G
ψ Yaw angle
$F_{x,A}$ Longitudinal force of the front wheel
$F_{x,PR}$ Longitudinal force of the rear right wheel
$F_{x,PL}$ Longitudinal force of the left wheel
$F_{y,A}$ Lateral force of the front wheel
$F_{y,PR}$ Lateral force of the rear right wheel
$F_{y,PL}$ Lateral force of the rear left wheel
$F_{z,A}$ Vertical force of the front wheel
$F_{z,PR}$ Vertical force of the rear right wheel
$F_{z,PL}$ Vertical force of the rear left wheel
X, Y, Z Components of the wind thrust in the vehicle reference frame
R_m Motion resistance
h_G Center of mass height
p, q, r Coordinates of the CoE in the vehicle reference frame
i_n Attack angle

INTRODUCTION

Land sailing refers to the motion across ground of a wheeled vehicle propelled by wind through the use of a sail. The term

[*]Address all correspondence to this author.

comes from analogy with (water) sailing. The first historical example of wind-powered vehicles can be traced back to China in 552 AD [1]. However, the precursor to the modern land-yacht was invented in 1600 by the Flemish scientist Simon Stevin in Flanders for recreation purposes [2]. In 1900, Louis Blériot contributed to develop land sailing as a popular sport and in 1967, the first "big" land-yacht race was organized by a French Foreign Legion officer along a 2700 km path across the Sahara Desert [3]. Another variation of the land-yacht is the Whike, [4], which combines land sailing with cycling and it can, therefore, be used in absence of wind, for example in urban environments.

A large body of research has been devoted to improve the performance of vehicles featuring one or several flexible or rigid vertical wing-sails [5], [6], [7], [8]. The wing-sails have the shape of an airfoil, and installed on wheels/boat to be used in land/water. In principle, the airfoil can constantly produce a lift-force that can generate a higher vehicle velocity than its prevailing wind. For example, a speed of 203.1 km/h was recorded for a land-yacht in 2009 when wind speeds were fluctuating between 48 and 80 km/h [9].
The use of wind-propelled vehicles has also been proposed for planetary exploration by NASA [10], [11]. JPL as well developed wind-driven inflatable spherical robots for polar expedition [12].

This paper presents a model that describes the response of a land-yacht given the command input, i.e. steer angle and sail trim angle, and wind conditions. Emphasis is given to the study of the interaction between wind and sail that generates the forces that propel the vehicle. One of the challenges towards autonomous driving is to set a proper angle of attack against the relative wind in order to steer the land-yacht to a planned destination. Currently, the angle of wing-sail is manually adjusted by land sailors. Therefore, to develop autonomous wind-driven vehicles, it is necessary to evolve their steering mechanisms from manual to automatic. A dual-input "expert" system is proposed to address this issue.
Results obtained from extensive simulations are included to verify the model and investigate the vehicle performance in open-loop (locked commands) and closed-loop operations.

VEHICLE MODEL

In this section, the kinematic and dynamic model of a land-yacht is presented. In Fig. 1, it is shown the kinematic scheme of the vehicle. Let X_V, Y_V, Z_V, be the vehicle-body frame (V-frame) whose origin is assumed to coincide with the center of mass, G. With reference to the parameters introduced in the Nomenclature, and under the assumption of planar motion and small angles, the slip angles of the front wheel and rear left and rear right wheels can be obtained, respectively, as:

$$\alpha_A = \frac{v + \dot{\psi} a}{u} - \delta \tag{1}$$

$$\alpha_{PR} = \frac{v - \dot{\psi} b}{u + \dot{\psi} \frac{t}{2}} \tag{2}$$

$$\alpha_{PL} = \frac{v - \dot{\psi} b}{u - \dot{\psi} \frac{t}{2}} \tag{3}$$

The forces acting on the system are shown in the free-body diagrams of Fig. 2. Due to the interaction with the wind, a stress distribution is generated across the sail. It is assumed that the resultant force is applied directly to a single point of the foil, which is referred to as the aerodynamic Center of Effort CoE (see [13], and labeled as S in Fig. 2) and at which the total moment produced from all forces over the foil can be represented by a single force producing the same moment. In reality, the actual position of this CoE is a function of a set of parameters, including the way in which the sail is trimmed, but we will ignore this effect and assume that the position of S remains constant. The resultant force or wind thrust has three components, i.e., (X, Y, Z). The wind trust component X allows the land-yacht to overcome the motion resistances and accelerate.
By applying Newton law to the land-yacht under the assumptions of rigid bodies, small angles, negligible rolling resistance of the wheels (i.e., $F_{xA} = F_{xPR} = F_{xPL} = 0$), it gets

$$\begin{array}{l} x : -F_{yA}\delta + X + R_m = M(\dot{u} - \dot{\psi} v) \\ y : F_{yA} + Y + F_{yPL} + F_{yPR} = M(\dot{v} + \dot{\psi} u) \\ z : F_z + F_{zPL} + f_{zPR} + Z - Mg = 0 \\ M_x(G) : (F_{yPL} + F_{yA} + F_{yPR}) h_G + (F_{zPL} - F_{zPR}) \frac{t}{2} + Zq - Yr = 0 \\ M_y(G) : F_{yA}\delta h_G - F_{zA} a + (F_{zPL} + F_{zPR}) b + Xr - Zp = 0 \\ M_z(G) : F_{yA} a - (F_{yPL} + F_{yPR}) b + Yp - Xq = I\ddot{\psi} \end{array} \tag{4}$$

where the $i-th$ tire lateral force F_{yi} can be considered as proportional to the sideslip angle α_i for small α_i

$$F_{yi} = -C_\alpha \alpha_i \quad i = A, PR, PL \tag{5}$$

C_α being the lateral stiffness of the tire.
Equation (4) can be expressed as a function of the highest deriva-

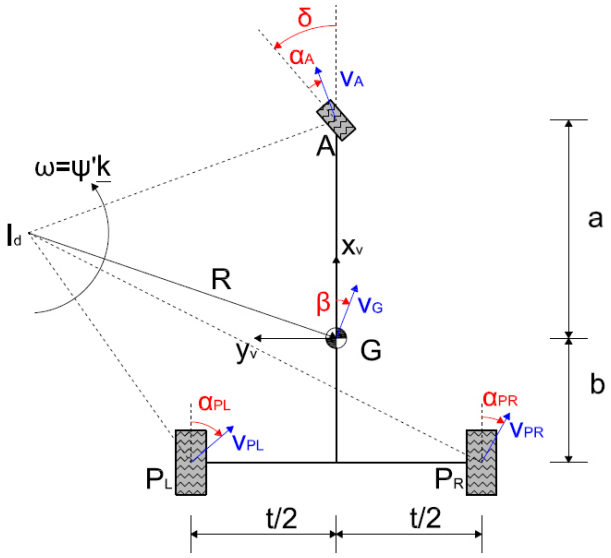

FIGURE 1. KINEMATIC MODEL FOR A THREE-WHEEL VEHICLE

tive

$$
\begin{aligned}
\dot{u} &= -\tfrac{F_{yA}\delta}{M} + \tfrac{X}{M} + \tfrac{R_m}{M} + \dot{\psi}v \\
\dot{v} &= \tfrac{F_{yA}}{M} + \tfrac{Y}{M} + \tfrac{f_{yPL}}{M} + \tfrac{f_{yPR}}{M} - \dot{\psi}u \\
\ddot{\psi} &= \tfrac{F_{yA}a}{I} - (F_{yPL+F_{yPR}})\tfrac{b}{I} + \tfrac{Yp}{I} - \tfrac{Xq}{I} \\
F_{zA} &= Mg - F_{zPL} - F_{zPR} - Z \\
F_{zPL} &= \tfrac{2Yr}{t} - 2\tfrac{Zq}{t} - 2(F_{yPL} + F_{yA} + F_{yPR})\tfrac{h_G}{t} + F_{zPR} \\
F_{zPR} &= \tfrac{Zp}{b} - \tfrac{Xr}{b} - \tfrac{F_{yA}\delta h_G}{b} + \tfrac{F_{zA}a}{b} - F_{zPL}
\end{aligned}
\tag{6}
$$

The motion of the land-yacht is governed by the first three differential equations of Eq. (6) that depend on the state variables (u, v, $\dot{\psi}$). The remaining equations are algebraic equations where the unknowns are the wheel vertical loads (i.e., F_{zA}, F_{sPR}, F_{zPL}).

VEHICLE AERODYNAMICS

With reference to Fig. 3, the true (absolute) wind speed, w, can be expressed in the inertial frame as

$$\mathbf{w} = \mathrm{w}\cos\gamma_t \mathbf{x_i} + \mathrm{w}\sin\gamma_t \mathbf{y_i} \tag{7}$$

where γ_t is the true wind angle. We are interested in the apparent (relative) wind, w_r, i.e., the vector difference of the true wind expressed in the vehicle reference frame and the yacht velocity, since the wind thrust is directly related to w_r. In addition, w_r should be referred to the CoE of the sail having coordinates $[p,q,r]^T$

$$\mathbf{w_r} = \mathbf{w} - \mathbf{V} - [0,0,\dot{\psi}]^T \times [p,q,r]^T \tag{8}$$

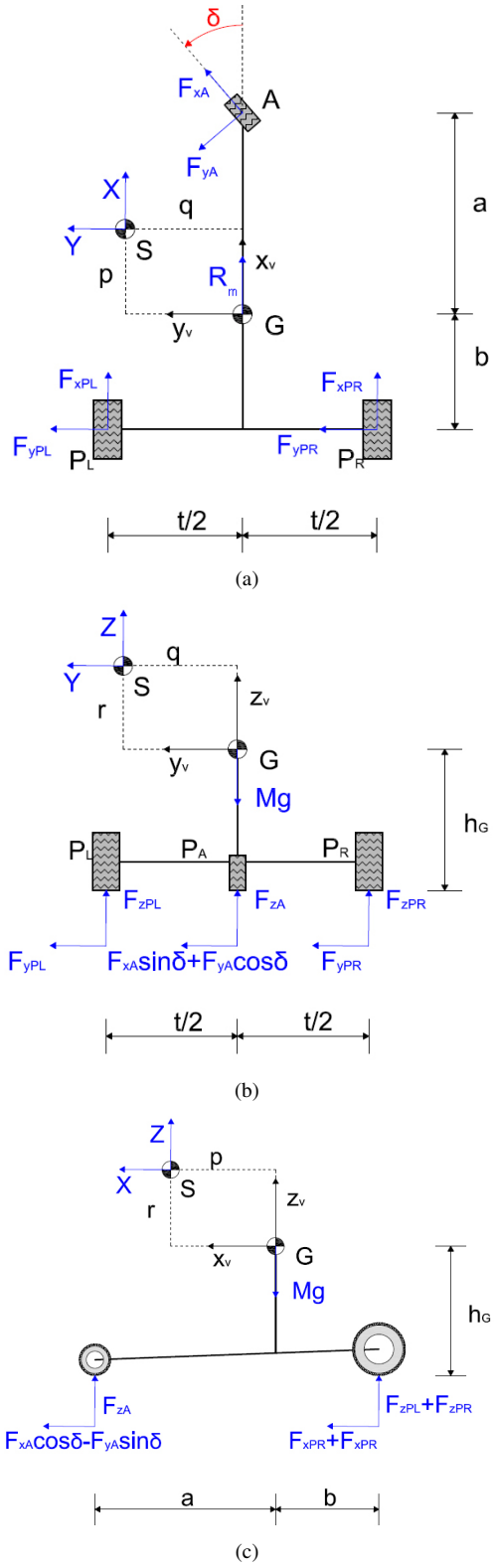

FIGURE 2. FORCES ACTING ON THE VEHICLE: (a) (X_V-Y_V PLANE), (b) (Y_V-Z_V PLANE), AND (c) (X_V-Z_V PLANE)

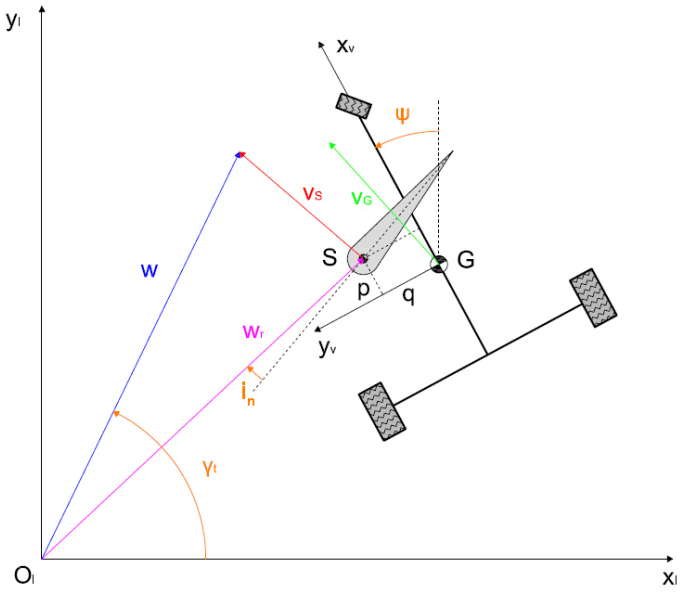

FIGURE 3. VEHICLE AERODYNAMICS

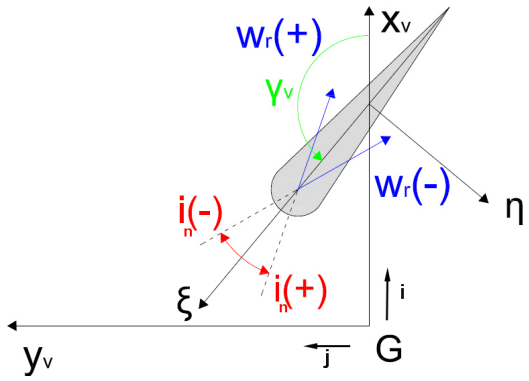

FIGURE 4. ATTACK ANGLE

Considering the components of w_r in the vehicle reference frame, it gets

$$\begin{aligned} w_{r,x} &= -w\cos(\gamma_t - \psi) - u + \dot{\psi} q \\ w_{r,y} &= -w\sin(\gamma_t - \psi) - v + \dot{\psi} p \end{aligned} \tag{9}$$

The wind thrust is also strongly influenced by the attack angle i_n, i.e. the angle between the chord line of the vertical airfoil and the relative wind velocity w_r, as explained in Fig. 4. With reference to the versors ξ and η of a reference frame attached to the sail, the attack angle can be defined as

$$\begin{aligned} i_n &= \pi - \arccos\left(\frac{w_r \xi}{|w_r||\xi|}\right) \quad if \quad w_r \cdot \eta < 0 \\ i_n &= -[\pi - \arccos\left(\frac{w_r \xi}{|w_r||\xi|p}\right)] \quad if \quad w_r \cdot \eta > 0 \end{aligned} \tag{10}$$

The attack angle is definite positive if counter-clockwise. In turn, the knowledge of i_n allows the lift and drag coefficients $C_L(i_n)$ and $C_D(i_n)$ to be defined. Experimental data referring to the symmetric NACA0012 profile used in this research can be found for example in [14] and they are reported in Fig. 5 for completeness. The corresponding lift and drag force can be obtained as

$$L = \frac{1}{2}\rho w_r^2 C_L(i_n) A \tag{11}$$

$$D = \frac{1}{2}\rho w_r^2 C_D(i_n) A \tag{12}$$

where A is the plan area of the vertical airfoil and ρ is the air density. L and D can be projected in the vehicle reference frame

$$\begin{aligned} \mathbf{L} &= L_x\mathbf{i} + L_y\mathbf{j} = L\left(-\frac{w_{ry}}{\sqrt{w_{rx}^2+w_{ry}^2}}\mathbf{i} + \frac{w_{rx}}{\sqrt{w_{rx}^2+w_{ry}^2}}\mathbf{j}\right) \\ \mathbf{D} &= D_x\mathbf{i} + D_y\mathbf{j} = L\left(-\frac{w_{rx}}{\sqrt{w_{rx}^2+w_{ry}^2}}\mathbf{i} + \frac{w_{ry}}{\sqrt{w_{rx}^2+w_{ry}^2}}\mathbf{j}\right) \end{aligned} \tag{13}$$

Finally, an expression of the aerodynamics forces can be drawn directly in the vehicle reference frame

$$\begin{aligned} X &= L_x + D_x \\ Y &= L_y + D_y \end{aligned} \tag{14}$$

In addition, the drag offered by the vehicle's body, F_{DB}, and wheels, F_{DW}, should also be taken into account as

$$R_m = F_{DB} + F_{DW} = -\frac{1}{2}\rho v_{aw,x}^2 C_{DB} A_B - B_W(n_f + 2n_r) \tag{15}$$

C_{DB} and A_B being, respectively, the vehicle fuselage drag coefficient and front area, B_W the drag coefficient of rolling wheel and n_f and n_r, respectively, the angular velocity of front and rear wheels.

SIMULATION RESULTS

In this section, it is studied the vehicle response in terms of tire slip angles, vertical loads, lateral forces, path, vehicle slip-angle, to different command input, i.e. steer angle and sail trim angle, and environment conditions, i.e. true wind intensity and angle. The parameters used in the simulations are collected in Table 1.

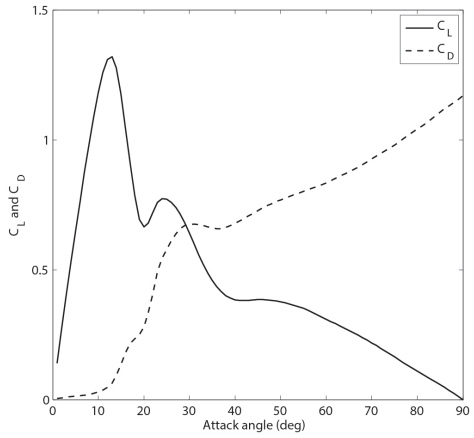

FIGURE 5. C_L AND C_D AS A FUNCTION OF THE ATTACK ANGLE FOR A NACA0012 WING

LOCKED COMMANDS

First, a simulation is performed with locked steer angle ($\delta = 0$ deg) and sail trim ($\gamma_v = 135$ deg), and starting longitudinal speed of $u = 1$ m/s and yaw angle $\psi = 0$ rad. True wind speed and angle are assumed constant, i.e. w = 5 m/s and $\gamma_t = 70$ deg. Figure 6 shows a snapshot of the vertical airfoil configuration at the beginning of the simulation. The velocity triangle that shows the relationship between the true wind speed, w, the vehicle speed, u, and the relative wind velocity, w_r, is shown in the bottom of Figure 6. It results in a positive attack angle of about 20 deg that generates a lift force, L, larger than the drag force, D. The resultant force F can be projected in the vehicle reference frame resulting in a component X that propels the vehicles and a component Y that acts as a lateral disturbance.

As the vehicle accelerates, the attack angle decreases, as shown in Figure 7(a), and the corresponding propulsion thrust X (Figure 7(b)) slightly increases as i_n rises up to the stall angle and then drops asymptotically. The vehicle reaches equilibrium at a constant velocity of $u = 2.8$ m/s (Figure 7(c)) when the the propulsion thrust balances the motion resistance. Due to the lateral disturbance Y, the vehicle drifts left, as shown by the path in Figure 7(d).

Finally, it is interesting to look at the vertical load acting on each tire of the land-yacht, as shown in Figure 8. Lateral weight shift can be observed at the beginning of the manoeuver due to the increase in Y, whereas it decreases as the vehicle approaches stationary state.

CONTROL OF THE LAND-YACHT

In order to increase the degree of autonomy of the land-yacht towards a robotic embodiment of the vehicle, a control system should be implemented. Two control input can be considered, i.e., the steer angle δ and the sail trim angle γ_v. Heading control is performed operating on δ, where the objective is to track the vehicle yaw ψ around a chosen set-point. It is assumed that the vehicle is equipped with a gyroscope providing the necessary feedback. Model-based approaches or optimal theory may be applied to this problem. However, here a PID strategy is used for simplicity. The objective of the sail angle controller is instead to optimize the aerodynamic behaviour of the system along a fixed path, preventing, for example, from up-wind conditions or helping the vehicle during tack/gybe maneuvers. A PID strategy is used for the sail angle controller as well. Sensor feedback are the vehicle speed and the wind properties.

TABLE 1. LAND-YACHT PARAMETERS USED IN THE SIMULATIONS

Parameter	Symbol	Value
Mass	M	100 kg
Rotational Inertia	I	30 kgm^2
Front pitch	a	1.05 m
Rear pitch	b	0.6 m
Rear width	t	1.4 m
G height	h_g	0.3 m
CoE height	r	1.7
Sail area	A_v	2 m^2
Sail chord	c	0.66 m
Front tire diameter	D_A	0.25 m
Rear tire diameter	D_P	0.35 m
Front cornering stiffness	C_A	200 N/m
Rear cornering stiffness	C_P	500 N/m
Fuselage drag coefficient	C_{DB}	0.473
Fuselage front area	A_B	0.25 m^2
Tire drag coefficient	B_w	0.0216 Ns

STRAIGHT PATH Using locked commands, it was shown in Fig. 6(d) that the vehicle drifts left. However, lateral drift can be compensated using steer control. For the same wind conditions (i.e., w = 5 m/s and γ_v=135 deg) and with reference to Fig. 9(a) the vehicle follows an approximately straight line using

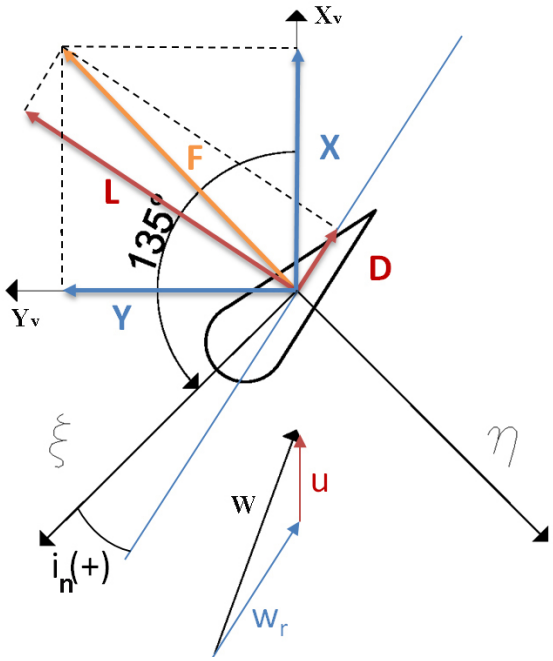

FIGURE 6. VELOCITY TRIANGLE AND CORRESPONDING AERODYNAMIC FORCES ON THE VEHICLE VERTICAL FOIL

heading control (blue line) in contrast to locked commands (red line). The controlled variable δ is shown in Fig. 9(b). Note that in this first simulation the sail trim control is off.

If the sail trim control is also active, the vehicle response is shown in Fig. 10. Now, γ_v is regulated in order to ensure an attack angle near the stall point (i.e., i_n =12deg) that maximizes the lift force. Figure 10(a) shows a comparison between the longitudinal speed obtained with full control and that reached with steer control only. It is apparent that the full control outperforms the partial control.

CLOSED PATH A second simulation is performed by controlling the land-yacht to follow an approximately oval path counter-clockwise. Along its course, the vehicle performs two 180-deg turns: one tacking and one gybing. Environment conditions are assumed constant with moderate wind blowing perpendicular to the vehicle along the straights, i.e. w = 4 m/s and γ_t= 0 deg. In the turns, the sail controller nulls out the attack angle to avoid up-wind conditions as the vehicle moves by inertia. Results are shown in Fig. 11, in terms of path, longitudinal speed and attack angle. As expected, the land-yacht slows down during the first tacking (at about 20 s) as the attack angle is nulled out (Fig. 11(c)). At the end of the left straight longitudinal speed reaches about 11 m/s that is more than double than the prevailing wind. The second turning motion is usually refereed to as a gybe (at about 52 s) with the vehicle moving from a starboard

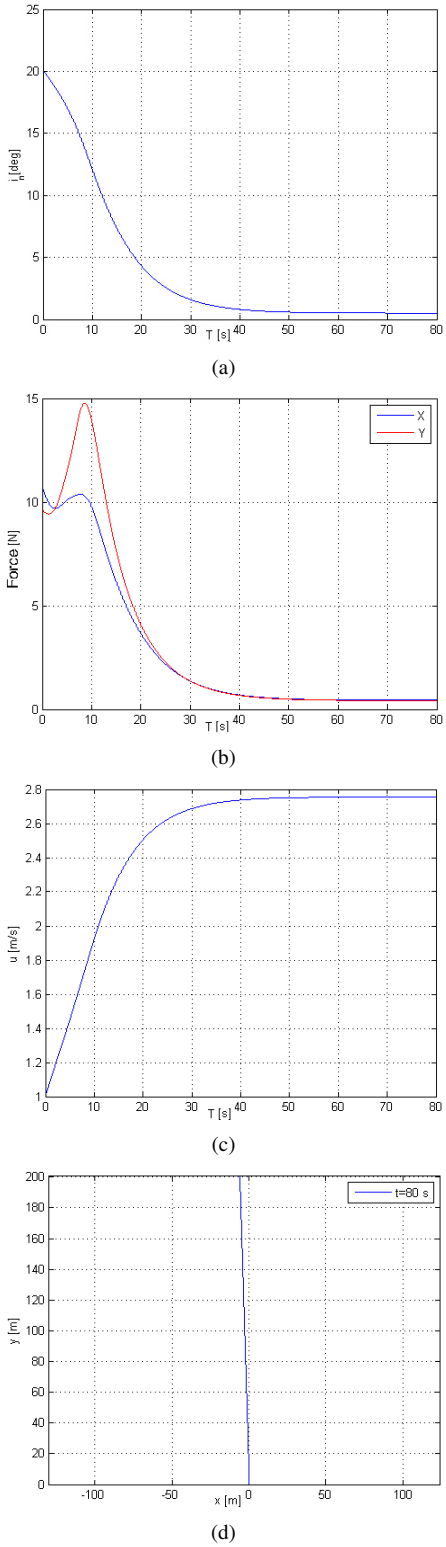

FIGURE 7. LAND-YACHT RESPONSE IN TERMS OF: (a) ATTACK ANGLE, (b) AERODYNAMIC FORCES, (c) LONGITUDINAL SPEED, AND (d) PATH

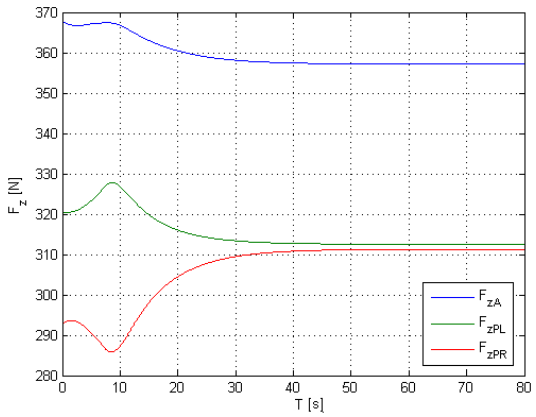

FIGURE 8. TIRE VERTICAL FORCES

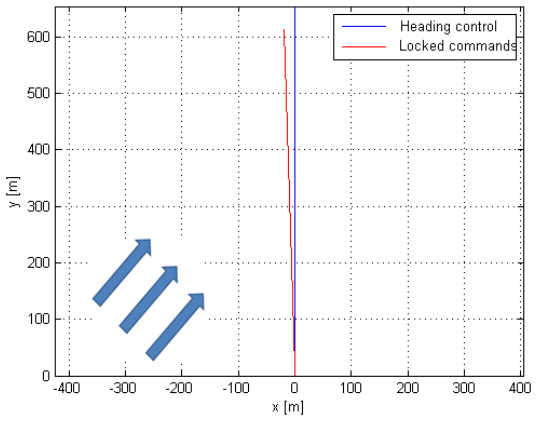

(a)

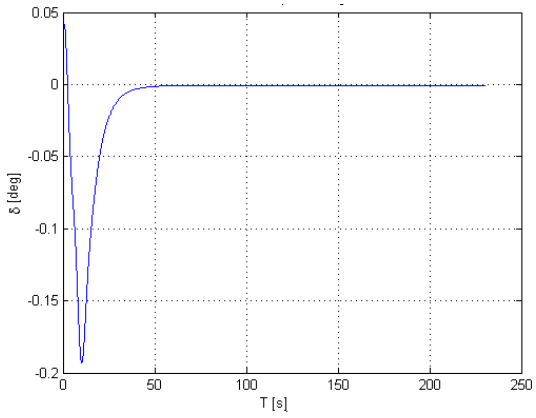

(b)

FIGURE 9. HEADING CONTROL: (a) PATH, and (b) STEER ANGLE

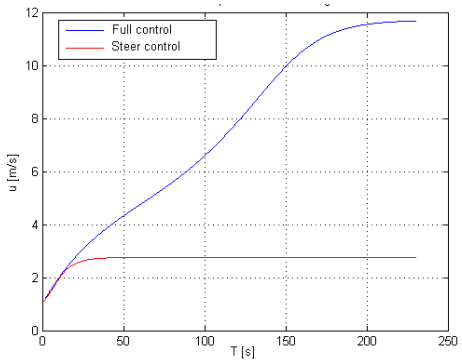

(a)

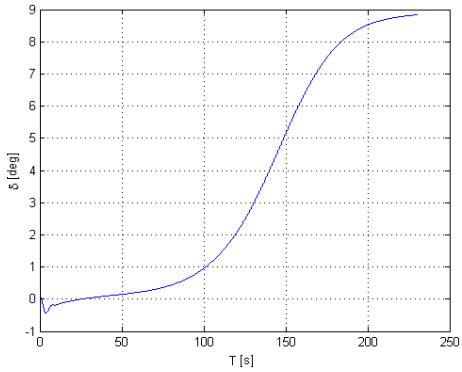

(b)

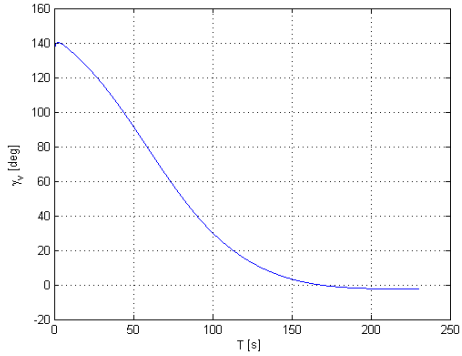

(c)

FIGURE 10. HEADING AND SAIL CONTROL: (a) LONGITUDINAL SPEED, (b) STEER ANGLE, (c) TRIM ANGLE

wind condition to a port wind condition resulting in an abrupt deceleration.

CONCLUSIONS

In this paper, the model of a wind-driven vehicle was presented. The land-yacht uses a vertical airfoil whose orientation is appropriately controlled to generate a lift that propels the vehicle. An additional control input is provided by the front steer angle

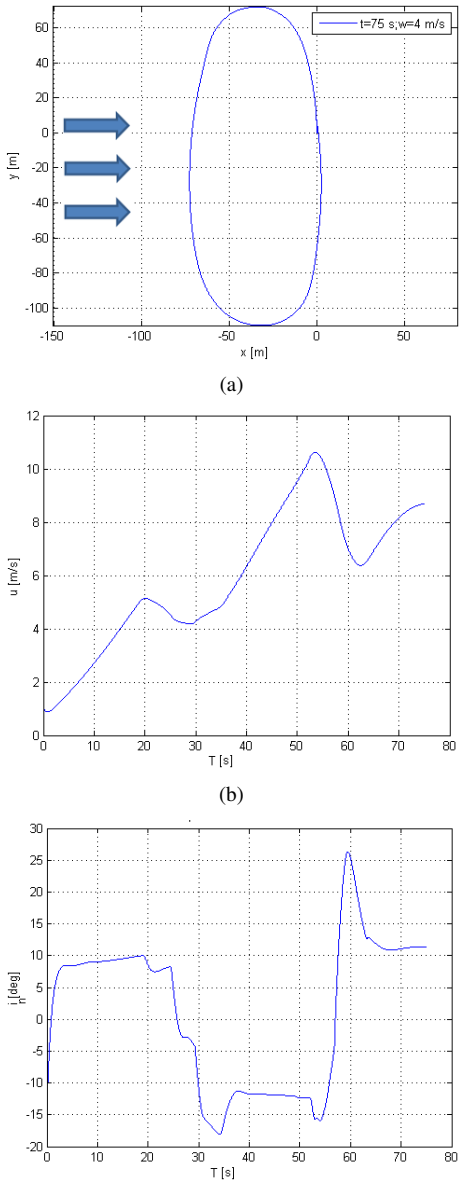

FIGURE 11. (a) CLOSED PATH, (b) LONGITUDINAL SPEED, (c) ATTACK ANGLE

to change heading. Extensive simulation results were included to analyze the vehicle response and performance to different wind conditions and control input, verifying the model and the feasibility of the proposed propulsion system.

ACKNOWLEDGMENT

The financial support of the ERA-NET ICT-AGRI2 through the grant Simultaneous Safety and Surveying for Collaborative Agricultural Vehicles (S3-CAV) is gratefully acknowledged.

REFERENCES

[1] Temple, R., 2007. *The Genius of China: 3,000 Years of Science, Discovery, and Invention*. Inner Traditions, New York, NY, USA.

[2] Devreese, J. T., and Vanden Berghe, G., 2008. *Magic is No Magic*. WIT Press, Amsterdam.

[3] Ligue Aquitaine Poitou Charentes de Char a Voile, 2016. Histoire du char voile. On the WWW, April. URL `http://www.charsavoile.fr/histl.htm`.

[4] Whike, 2016. On the WWW, April. URL `http://whike.com/en/`.

[5] Walker, J., 1996. "A high performance automatic wing sail auxiliary propulsion system for commercial ships". *J. Wind Eng. Ind. Aerodyn.,* ***20***(3), pp. 83–96.

[6] Van Oossanen, P., 1993. "Predicting the speed of sailing yachts". *Trans. Soc. Naval Arch. Mar. Eng.,* ***101***, pp. 337–397.

[7] Yoo, J., and Kim, H., 2006. "Computational and experimental study on performance of sails of a yacht". *Ocean Eng.,* ***33***, pp. 1322–1342.

[8] Mirzaei, P. A., and Rad, M., 2013. "Toward design and fabrication of wind-driven vehicles: Procedure to optimize the threshold of driving forces". *Applied Mathematical Modelling,* ***37***(1–2), pp. 50–61.

[9] BBC, 2009. Wind-powered car breaks record. On the WWW, March. URL `news.bbc.co.uk/2/hi/technology/7968860.stm`.

[10] Hajos, G., Jones, J., and Behar, A., 2005. "An overview of wind-driven rovers for planetary exploration". In AIAA Aerospace Sciences meeting and exhibit, pp. 1–13.

[11] Benigno, G., Motiwala, S., Landis, G., and Colozzo, A., 2013. "A wind-powered rover for a low-cost Venus mission". In AIAA Aerospace Sciences Meeting, pp. 1–22.

[12] Behar, A., Carsey, F., Matthews, J., and Jones, J., 2004. "An antarctic deployment of the nasa/jpl tumbleweed polar rover". In Automation Congress, 2004. Proceedings. World, Vol. **15**, pp. 453–460.

[13] Fossen, T., 1994. *Guidance and Control of Ocean Vehicles*. Wiley, New York, NY, USA.

[14] Khayyata, M., and Rad, M., 2009. "Some experimental studies on the performance of a rigid wing land yacht model in comparison with vpp". *Scientia Iranica,* ***16***(4), May, pp. 291–300.